A Parallel Coiled-Coil Tetramer with Offset Helices[†,‡]

Jie Liu,[§] Yiqun Deng,[§] Qi Zheng,[§] Chao-Sheng Cheng,[§] Neville R. Kallenbach,[||] and Min Lu*[,§]

Department of Biochemistry, Weill Medical College of Cornell University, New York, New York 10021, and Department of Chemistry, New York University, New York, New York 10003

Received September 14, 2006; Revised Manuscript Received October 17, 2006

ABSTRACT: Specific helix−helix interactions are fundamental in assembling the native state of proteins and in protein−protein interfaces. Coiled coils afford a unique model system for elucidating principles of molecular recognition between α helices. The coiled-coil fold is specified by a characteristic seven amino acid repeat containing hydrophobic residues at the first (*a*) and fourth (*d*) positions. Nonpolar side chains spaced three and four residues apart are referred to as the 3-4 hydrophobic repeat. The presence of apolar amino acids at the *e* or *g* positions (corresponding to a 3-3-1 hydrophobic repeat) can provide new possibilities for close-packing of α-helices that includes examples such as the *lac* repressor tetramerization domain. Here we demonstrate that an unprecedented coiled-coil interface results from replacement of three charged residues at the *e* positions in the dimeric GCN4 leucine zipper by nonpolar valine side chains. Equilibrium circular dichroism and analytical ultracentrifugation studies indicate that the valine-containing mutant forms a discrete α-helical tetramer with a significantly higher stability than the parent leucine-zipper molecule. The 1.35 Å resolution crystal structure of the tetramer reveals a parallel four-stranded coiled coil with a three-residue interhelical offset. The local packing geometry of the three hydrophobic positions in the tetramer conformation is completely different from that seen in classical tetrameric structures yet bears resemblance to that in three-stranded coiled coils. These studies demonstrate that distinct van der Waals interactions beyond the *a* and *d* side chains can generate a diverse set of helix−helix interfaces and three-dimensional supercoil structures.

Coiled coils consist of two or more α-helices that interwind in a left-handed supercoil (*1*, *2*). Coiled-coil sequences in proteins commonly share a seven-amino acid sequence, the 3-4 heptad repeat, the positions in which are denoted by letters *a* to *g* (*3*). The first (*a*) and fourth (*d*) positions are predominantly occupied by hydrophobic residues such as Leu, Ile, Val, and Ala, whereas amino acids at positions *e* and *g* are frequently polar or charged (*3*−*6*). The interacting surface between supercoiled α-helices is formed by complementary "knobs-into-holes" packing of the *a* and *d* side chains (*7*, *8*); this arrangement represents an essential structural feature of the coiled-coil family (*2*, *9*). Beyond the fundamental role of apolar residues at the core *a* and *d* positions, interhelical electrostatic interactions between the flanking *e* and *g* positions specify interchain interactions (*10*−*15*). For example, repulsive or attractive interactions between the *e* and *g* side chains can produce a high level of conformational selectivity for heterodimers *versus* homodimers (*10*, *11*, *16*−*18*). These characteristics of the 3-4 heptad repeat have stimulated development of bioinformatics programs to predict coiled-coil domains in protein sequences (*4*, *19*−*24*).

The coiled-coil motif has also served as a unique model system for studying protein folding (*25*, *26*), molecular recognition (*10*, *27*), and *de novo* protein design (*28*−*31*). Plasticity in coiled-coil structure includes changes in oligomeric state, strand polarity, homo- *versus* heteromeric association, heptad register of helices, and the presence or absence of cavities or channels enclosed by the helices (*2*). Helix-packing interactions are sensitive to the geometric properties of the core *a* and *d* residues, as well as effects exerted by the *e* and *g* side chains (*9*). Incisive studies by Harbury et al. (*32*, *33*) on the 33-residue GCN4 leucine-zipper dimerization domain revealed a crucial role for interior packing of the *a* and *d* side chains in dictating the stoichiometry of parallel coiled-coil conformations. For example the presence of isoleucine in position *a* and leucine in *d* promotes dimer formation, while the reverse arrangement favors tetramers instead. On the other hand, isoleucines at both *a* and *d* positions define trimers. Moreover, a single polar asparagine side chain at an *a* position plays a pivotal role in specifying dimeric structure by forming a buried interhelix hydrogen bond (*32*, *34*−*37*).

Accurate prediction of side chain packing and its influence on tertiary conformation is an enduring objective for modern protein structural analysis and design efforts. Engineering of novel coiled-coil interfaces has been used to test and enhance our growing ability to predict folded structures (*30*, *31*, *38*). A number of experimental results based on natural as well as designed coiled coils reveal that van der Waals

[†] This work was supported by National Institutes of Health Grant AI042382 and by the Irma T. Hirschl Trust. Partial support for C.-S.C. was provided by a fellowship from National Science Council (Taiwan).

[‡] The atomic coordinates and structure factors have been deposited in the RCSB Protein Data Bank (entry 2IPZ).

* Corresponding author. Phone: (212) 746-6562. Fax: (212) 746-8875. E-mail: mlu@med.cornell.edu.

[§] Weill Medical College of Cornell University.

[||] New York University.

10.1021/bi061914m CCC: $33.50
Published on Web 11/29/2006

interactions between apolar side chains at the *e* and *g* positions are an important determinant of the global three-dimensional architecture (*11*, *31*, *39*−*50*). So-called "3-3-1" hydrophobic heptad repeats containing nonpolar amino acids at the *a*, *d*, *e* or *a*, *d*, *g* positions have been found to encode stable antiparallel four-helix structures with combined knobs-against-knobs and knobs-into-holes packing of the three hydrophobic side chains (*42*, *46*, *49*, *50*). Antiparallel tetramer configurations with alanine at the *e* or *g* positions have been classified into two distinct types of tightly packed helix arrangements, referred to as "Alacoils" (*51*). In one, the ferritin type, the helices are staggered by 0.25 heptad (*42*, *49*). In the second, the rop type, the helices are shifted by 0.5 heptad (*50*, *52*). This potential to shift heptad register presents an additional element of conformational plasticity in coiled coils, as we noted above.

We have previously characterized variants of the GCN4 leucine-zipper dimer that adopt antiparallel tetrameric structures in response to hydrophobic substitutions at the *g* positions (*46*). Unexpectedly we have found that a leucine-zipper mutant with alanine residues at both the *e* and *g* positions forms a parallel heptamer, suggesting that much remains to be learned about the principles of coiled-coil assembly (*45*). Here we investigate *a*, *d*, *e* packing interactions using a leucine-zipper peptide in which nonpolar valine side chains replace three charged amino acids at the *e* positions. Structural and biophysical analysis of the valine-containing mutant reveals a previously uncharacterized type of parallel four-stranded coiled coil with extended knobs-into-holes packing interactions based on pairs of associating trimers rather than tetramers. Although at this point we have only begun systematic studies of the diversity of interhelical packing interactions in coiled-coil structures, we can conclude that the 3-3-1 hydrophobic residue repeat engenders new folds that merit investigation as has the canonical 3-4 heptad repeat thus far.

MATERIALS AND METHODS

Protein Expression and Purification. The GCN4-pVe peptide was expressed in *Escherichia coli* strain BL21(DE3)/pLysS using a modified pET3a vector (Novagen, Madison, WI). Substitutions were introduced into the GCN4-pR plasmid (*53*) using the method of Kunkel (*54*) and verified by DNA sequencing. Cells were grown at 37 °C in Luria−Bertani (LB[1]) media to an optical density of 0.6 at 600 nm and induced with isopropylthio-β-D-galactoside (IPTG) for 3 h at 37 °C. Cells were lysed at 0 °C by glacial acetic acid and centrifuged (35000*g* for 30 min) to separate the soluble fraction from inclusion bodies. The soluble fraction was subsequently dialyzed into 5% acetic acid overnight at 4 °C. Peptides from the soluble fraction were purified to homogeneity by reverse-phase high-performance liquid chromatography (HPLC) on a C18 preparative column using a water−acetonitrile gradient in the presence of 0.1% trifluoroacetic acid and lyophilized. Peptide identities were confirmed by electrospray mass spectrometry (PerSeptive Biosystems Voyager Elite, Cambridge, MA). Protein concentrations were determined by using the method of Edelhoch (*55*).

Circular Dichroism Spectropolarimetry. CD spectra were measured on an AVIV 62A/DS spectropolarimeter (Aviv Associate, Lakewood, NJ) equipped with a thermoelectric temperature control in 50 mM Tris-HCl (pH 8.0) and 150 mM NaCl (TBS) and 200 μM peptide. The wavelength dependence of molar ellipticity, $[\theta]$, was monitored at 0 °C as the average of five scans using a 5 s integration time at 1.0 nm wavelength increments. Spectra were baseline-corrected against the cuvette with buffer alone. Helix content was estimated from the CD signal by dividing the mean residue ellipticity at 222 nm by the value expected for 100% helix formation by helices of comparable size, −33,000 deg cm^2 dmol^{-1} (*56*). Thermal stability was determined by monitoring the change in $[\theta]_{222}$ as a function of temperature, and thermal melts were performed in 2° intervals with a 2 min equilibration at the desired temperature and an integration time of 30 s. Reversibility was verified by repeated scans. Superimposable folding and unfolding curves were observed, and >95% of the signal was regained upon cooling. Values of midpoint unfolding transitions (T_m) were estimated by evaluating the maximum of the first derivative of $[\theta]_{222}$ *versus* temperature data (*57*).

Analytical Ultracentrifugation. Sedimentation equilibrium experiments were performed on a Beckman XL-A analytical ultracentrifuge (Fullerton, CA) equipped with an An-60 Ti rotor at 20 °C as described (*58*). Protein solutions were dialyzed overnight against TBS (pH 8.0), loaded at initial concentrations of 50, 200, and 800 μM, and analyzed at rotor speeds of 25 and 28 krpm. Data were acquired at two wavelengths per rotor speed setting and processed simultaneously with a nonlinear least-squares fitting routine (*59*). Solvent density and protein partial specific volume were calculated from the solvent and protein composition, respectively (*60*). Apparent molecular masses were all within 10% of those calculated for an ideal tetramer with no systematic deviation of the residuals.

Crystallization and X-ray Data Collection. Crystals of GCN4-pVe were grown from 15 mg/mL HPLC-purified peptide in water, 0.1 M HEPES-Na (pH 7.8), 10% (vol/vol) isopropanol, 0.1 M NaBr, 20% PEG 4000 at room temperature. Crystals belong to space group $P2_1$ (a = 23.7 Å, b = 53.9 Å, c = 52.0 Å, β = 95.8°) and contain four monomers in the asymmetric unit, with a solvent content of 45.4%. The crystals were transferred into a cryosolution containing 0.1 M HEPES-Na (pH 7.8), 10% isopropanol, 0.1 M NaBr, 25% PEG 4000, 15% glycerol and frozen in liquid nitrogen. Diffraction data were recorded at 100 K on a MAR345 image plate at the beamline X4C of the National Synchrotron Light Source at Brookhaven National Laboratory. The images were indexed and integrated with the programs DENZO and SCALEPACK (*61*). Data collection statistics are presented in Table 1.

Structure Determination and Refinement. The structure of GCN4-pVe was solved by molecular replacement with the program Phaser (*62*) using the GCN4-pV monomer structure (PDB entry 2B22) as a search model. This model and the dataset for GCN4-pVe were directly fed to the program Arp/Warp (*63*), which provided a largely complete asymmetric unit of four chains and allowed ~91% of the final model to be interpreted. The resulting experimental electron density

[1] Abbreviations: LB, Luria−Bertani; IPTG, isopropylthio-β-D-galactoside; HPLC, high-performance liquid chromatography; CD, circular dichroism; TBS, Tris-buffered saline; GuHCl, guanidine hydrochloride; $[\theta]_{222}$, molar ellipticity at 222 nm; T_m, midpoint of the thermal unfolding transition; rms, root-mean-square.

Table 1: Crystallographic Data and Refinement Statistics

Data Collection	
resolution (Å)	52.0−1.35
unique reflections	27103
redundancy	3.4 (3.7)[a]
completeness (%)	94.5 (95.3)
R_{merge} (%)[b]	4.7 (39.5)
$I/\sigma(I)$	17.5 (4.9)
space group	$P2_1$
unit-cell parameter	$a = 23.7$ Å, $b = 53.9$ Å, $c = 52.0$ Å, $\beta = 95.8°$
molecules in the asymmetric unit	4
solvent content (%)	45.4
Refinement	
resolution (Å)	52.0−1.35
reflections	27 103
protein atoms	1116
water molecules	164
R_{cryst}/R_{free} (%)[c]	20.2/23.7
average temperature factors (Å^2)	20.3
RMS Deviations from Ideal Geometry	
bond lengths (Å)	0.01
bond angles (deg)	1.3
torsion angles (deg)	4.1
B values (Å^2)	1.0

[a] Values in parentheses refer to the highest resolution shell (1.35−1.37 Å). [b] $R_{merge} = \sum|I - \langle I\rangle|/\sum I$, where I is the integrated intensity of a given reflection. [c] $R_{cryst} = \sum|F - F_c|/\sum F_o$, $R_{free} = R_{cryst}$ calculated using 10% of the reflection data chosen randomly and omitted from the start of refinement.

map was of excellent quality and showed the location of most of the side chains. Crystallographic refinement of the GCN4-pVe structure was carried out using Refmac (*64*) in CCP4i program suite (*65*). Density interpretation and manual model building were done with the program O (*66*). An overall anisotropic thermal factor correlation was applied by using TLS groups for each monomer (*67*). The final model ($R_{cryst} = 20.2\%$ and $R_{free} = 23.7\%$ for the resolution range 52.0−1.35 Å) includes 136 amino acids of the tetramer, one isopropanol, one glycerol, and 164 water molecules. The model exhibits root-mean-square (rms) deviations from ideal bond lengths and bond angles of 0.01 Å and 1.3°, respectively. All protein residues are in the most preferred regions of the Ramanchandran plot.

Structure Analysis. Coiled-coil parameters were calculated with the program TWISTER (*68*). Residues 6−32 of GCN4-pVe were used in the calculations. The rms deviations were calculated with LSQKAB in the CCP4i program suite (*65*). Buried surface areas were calculated from the difference of the accessible side chain surface areas of the tetramer structure and of the individual helical monomers using CNS 1.0 (*69*). Residues 1−34 of GCN4-pVe and residues 1−33 of GCN4-pLI were used in the calculations. Atomic solvation energy was calculated using the method of Eisenberg and McLachlan (*70*). The net solvation energies were derived by subtracting the energies of the component α-helices from the energy of the oligomer structure. Residues 5−31 of the GCN4-pVe tetramer and the GCN4-pMSE dimer (*53*) were used in the calculations; the four most N-terminal residues and the three most C-terminal residues of GCN4-pVe and GCN4-pMSE were omitted from the calculation to minimize end effects. Figures were generated using SETOR (*71*), Insight II (Accelrys, San Diego, CA), and GRASP (*72*).

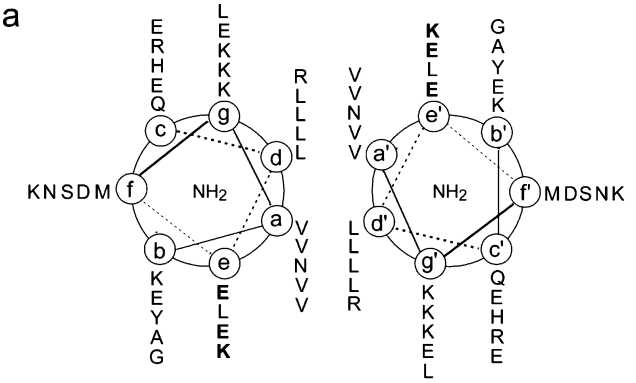

FIGURE 1: Position *e* mutant of the dimeric GCN4 leucine zipper. (a) Helical wheel projection of Met1 to Arg34 of the wild-type GCN4-pR peptide. The view is from the N terminus. Heptad-repeat positions are labeled *a* through *g*. Prime (′) refers to positions from the second helix. Three charged residues at position *e* are highlighted in bold. The GCN4-pR sequence contains an additional Met-Lys-Val and no Arg-Met at its N terminus but is otherwise identical with GCN4-p1. (b) The amino acid sequence of the GCN4-pVe peptide used in this study. Residues at positions *a* and *d* are underlined. The three charged *e* amino acids in wild-type GCN4-pR are replaced by nonpolar valine side chains.

RESULTS AND DISCUSSION

Position e Valine Mutant of the GCN4 Leucine Zipper. The dimeric GCN4 leucine zipper has offered a benchmark protein−protein interface with which to study the detailed relationships between local conformational interactions and overall coiled-coil architecture (*8*, *32*, *45*). The hydrophobic faces of the two α-helices of the classical dimer pack against each other in a parallel orientation (*8*); the interface formed engages residues at the *a*, *d*, *e*, and *g* positions of the heptad repeat (Figure 1a). Introduction of nonpolar side chains at the normally charged *g* positions into the canonical GCN4-pR sequence can switch both oligomerization state and strand polarity, leading to a stable tetramer in which the antiparallel helices shift by 0.5 heptad (*46*). Experimental analysis of the *lac* repressor tetramerization domain has revealed that residues at the *a*, *d*, and *e* positions in this antiparallel tetramer comprise the hydrophobic core, producing a helical offset of 0.25 heptad (*42*−*44*). The mechanism that determines helix register in these antiparallel structures remains incompletely understood. Given the apparent inequivalence of the *e* and *g* heptad positions, we decided to examine in more detail the role of the triad *a*, *d*, *e* pattern on the overall structure of the leucine-zipper model. We completely substituted three charged *e* amino acids in GCN4-pR with valine to generate the variant that we refer to as GCN4-pVe (Figure 1b).

GCN4-pVe Forms a Stable Four-Helix Bundle in Solution. On the basis of circular dichroism (CD) measurements in 50 mM Tris-HCl (pH 8.0) and 150 mM NaCl (TBS), GCN4-pVe is ∼90% helical at 0 °C and undergoes a cooperative thermal unfolding transition with a midpoint (T_m value) of greater than 88 °C at 200 μM peptide concentration (Figure 2a), compared with a T_m of 63 °C for the parent molecule GCN4-pR under the same conditions. Equilibrium analytical ultracentrifugation indicates that GCN4-pVe sediments as a discrete tetramer and exhibits no systematic dependence of

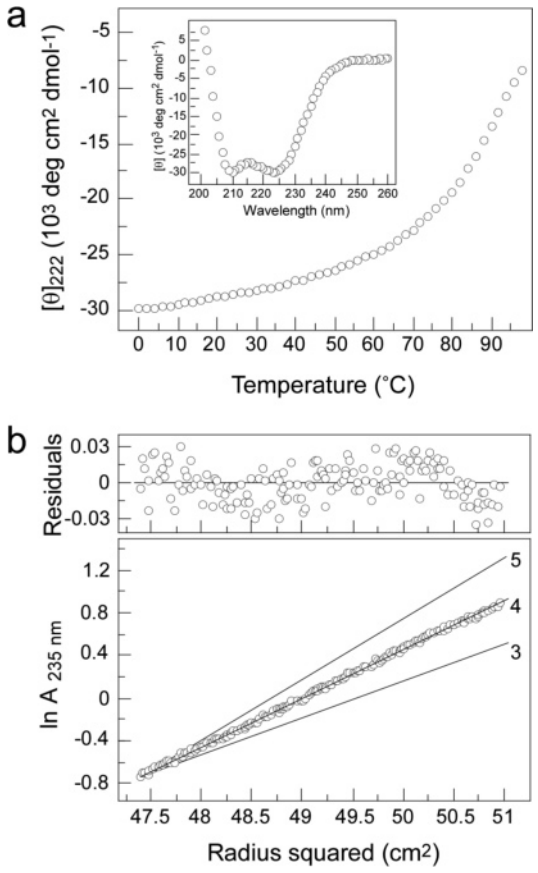

FIGURE 2: Folding of GCN4-pAe into a stable α-helical tetramer. (a) Thermal melt monitored by CD at 222 nm and 200 μM peptide in TBS (pH 8.0). (Inset) Circular dichroism spectrum at 0 °C. (b) Representative sedimentation equilibrium data for a 200 μM sample at 20 °C and 25 krpm in TBS (pH 8.0). The natural logarithm of the absorbance at 235 nm is plotted against the square of the radial position. Lines expected for trimeric and pentameric models are indicated for comparison. The deviation in the data from the linear fit for a tetrameric model is plotted (upper).

apparent molecular mass on peptide concentration from 50 μM to 800 μM (Figure 2b). Thus GCN4-pVe folds into a well-ordered, stable four-helix bundle.

Crystal Structure of the GCN4-pVe Tetramer. To investigate details of the interfacial *a*, *d*, and *e* side chain packing in this tetramer, we determined the X-ray crystal structure of the GCN4-pVe peptide at 1.35 Å resolution (Table 1). GCN4-pVe forms a unique parallel four-stranded coiled coil ~54 Å in length with a maximum diameter of 27 Å (Figure 3a and b). The adjacent helices A−B and C−D are vertically shifted from each other by three amino acids, resulting in an unusual layering effect of residues in the hydrophobic core of the tetramer (see below). The crossing angle between all four helix pairs is about 25°; the four helical monomers wrap tightly around the superhelical axis to form a gradual left-handed supercoil. In contrast to the parallel GCN4-pLI tetramer with a pitch value of 205 Å, the pitch of the GCN4-pVe supercoil is 162 Å (Table 2). This smaller pitch allows the *a*, *d*, and *e* side chains of the A and C helices (on diagonal) to face toward the axis of supercoil rotation and mesh as the four parallel α-helical chains interlock (Figure 3c−e). As a consequence, adjacent helices of the GCN4-pVe tetramer are separated by approximately the same distance as the A and C helices, while the B and D helices are 5.6 Å further apart. These interfacial interactions involving hydrophobic side chains at the *a*, *d*, and *e* positions are tighter than in the original dimer, consistent with the increased stability (see Figure 2a). This conclusion is in accord with the predicted gain of −8.0 kcal/mol in net hydrophobic stabilization energy (*70*) of the tetramer relative to the dimer structure.

Because the vertical translation of the A−B and C−D helices results in a displacement equivalent to 0.43 heptad, there is an approximate layering of *a*−*d* pairs with this helical offset value (Figure 3). In essence 16 *a* and *d* residues of the B and D chains pack against the 24 *a*, *d*, and *e* residues of the A and C chains to form the tetramer interface, which consists of eight hydrophobic layers (Figure 4). (Note that the Val3 residues of the A and B chains and the Val31 residues of the C and D chains create dimer *a* layers as overhangs of the GCN4-pVe tetramer.) Cross-sectional layers containing *d* leucines of helices A and B, *a* valines/asparagines of C and D, and *e* valine of helix A alternate with layers containing *d* leucines of helices C and D, *a* valines/asparagines of helices A and B, and *e* valine of helix C (Figure 3a). All the *a*, *d*, and *e* side chains (except for two leucines, two asparagines, and one valine) assume their most favored rotamers in α helices (*73*, *74*). Notably, the Leu20 residue of helix A adopts an unusual dihedral angle near 78°, 86°; this rotamer conformation appears to be necessary to achieve efficient van der Waals contacts with Asn17 of helix C and Leu20 of helix B, presumably because of the polar group of the Asn17 side chain.

"*Conjoined Trimer*" *Core Packing in GCN4-pVe*. The GCN4-pVe tetramer comprises two series of interlocking knobs-into-holes packing interactions between triads of the A−B−C and A−C−D chains (Figure 3b), a pattern that to our knowledge has not been reported before. In layers 2, 4, 6, and 8 (see Figure 3c), looking from the N terminus down the superhelix axis, knobs formed by *d* leucines of helix A pack into holes formed by the *d* and *e* side chains and two adjacent *a* layers of helix B; *d* knobs from helix B fit into holes by the *a* and *b* side chains and two adjacent *e* layers of helix C; and *a* knobs from helix C dock into holes by the *d* and *e* side chains and two adjacent *a* layers of helix A (we call this trimeric core packing the clockwise A−B−C *d*-*d*-*a* triad). In the cyclic complementary counterclockwise A−D−C *e*-*a*-*a* triad (Figure 3c), *e* knobs from helix A interact with holes formed by the *a* and *g* residues and two adjacent *d* layers of helix D; *a* knobs from helix D dock into holes by the *a* and *g* side chains and two adjacent *d* layers of helix C; and *a* knobs from helix C pack into holes by the *d* and *e* side chains and two adjacent *a* layers of helix A.

Similarly, in layers 3, 5, 7, and 9 (see Figure 3d), the knobs-into-holes interaction of the counterclockwise A−C−B *a*-*e*-*a* triad is coupled with that of the clockwise A−C−D *a*-*d*-*d* triad. Thus the *a*, *b*, *d*, *e*, and *g* residues of the A and C chains and the *a*, *d*, *e*, and *g* of the B and D chains segregate into four geometrically distinct helix−helix interfaces (Figures 3e and 4). Compared with the side chains of isolated helices, the *a*, *d*, and *e* residues of helices A and C, and the *a* and *d* residues of helices B and D are completely buried; the *b* and *g* residues of helices A and C, and the *e* and *g* residues of helices B and D are partly buried; and the *c* and *f* positions of helices A and D, and the *b*, *c*, and *f* positions of helices B and D remain completely exposed

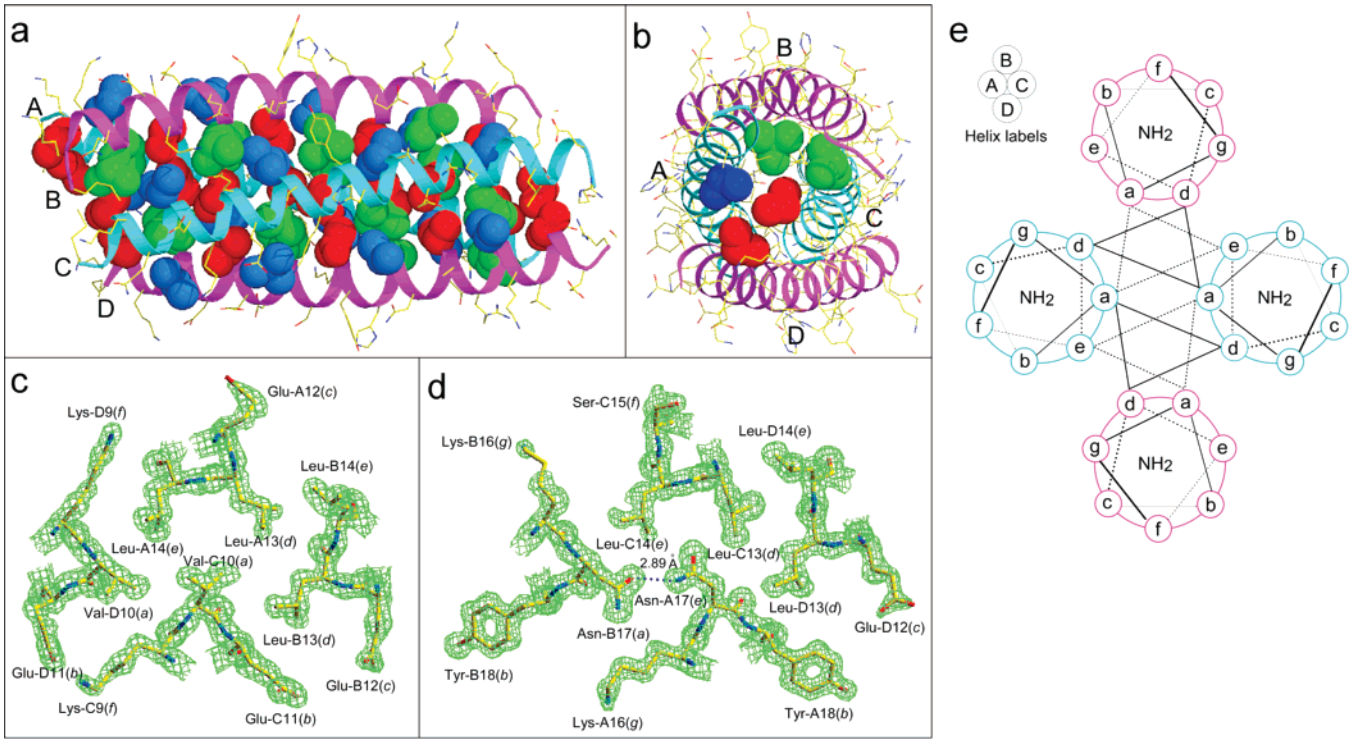

FIGURE 3: Crystal structure of the GCN4-pVe tetramer. (a) Lateral view of the parallel tetramer (residues 1−34). The GCN4-pVe backbone is shown in cyan and pink C_α representation for the A/C and B/D helices (labeled at the N terminus), respectively. Red van der Waals surfaces identify residues at the *a* positions, green surfaces identify residues at the *d* positions, and blue spheres identify residues at the *e* positions. (b) Axial view of the parallel tetramer. The view is from the N terminus looking down the superhelical axis. The van der Waals surfaces are colored red for the Val-C3(*a*) and Val-D3(*a*), green for Leu-A6(*d*) and Leu-B6(*d*), and blue for Val-A7(*e*). (c) Cross section of the tetramer in the Val-C10(*a*), Val-D10(*a*), Leu-A13(*d*), Leu-B13(*d*), and Val-A14(*a*) layer. The 1.35 Å $2F_o - F_c$ electron density map at 1.5σ contour is shown with the refined molecular model. (d) Cross section of the tetramer in the Leu-C13(*d*), Leu-D13(*d*), Val-C14(*e*), Asn-A17(*a*), and Asn-B17(*a*) layer. A hydrogen bond is denoted by a pink dotted line. (e) Schematic cross section through the parallel tetramer, depicting interhelical packing interactions between the *a*, *a*, and *e* side chains (dotted lines) and between the *a*, *d*, and *d* side chains (solid lines).

Table 2: Structural Parameters of Parallel Leucine-Zipper Coiled Coils

	GCN4 leucine-zipper variant[a]			
	p1 dimer	pII trimer	pLI tetramer	pVe tetramer
superhelix parameter				
supercoil radius, R_0 (Å)	4.9	6.7	7.6	6.7
residues per supercoil turn, ω_0	100	118	139	112
supercoil pitch (Å)	148	175	205	162
α-helix parameter				
residues per α-helix turn, *n*	3.62	3.60	3.59	3.62
rise per residue, *d* (Å)	1.51	1.53	1.52	1.51
α-helix radius (C_α), R_1 (Å)	2.28	2.24	2.26	2.29

[a] Values for the leucine-zipper peptide variants were from ref 33.

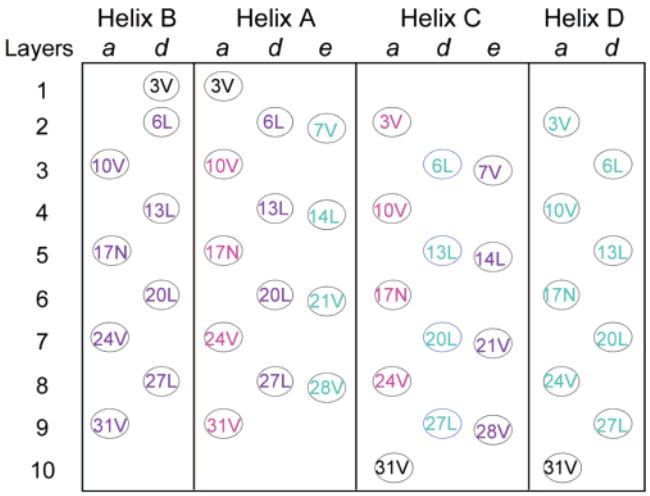

FIGURE 4: Core packing in the parallel GCN4-pVe tetramer. Helix cross-sectional layers centered in acute knobs-into-holes packing of the A−B−C (purple) and A−C−D (cyan) chains are shown. The eight valine side chains at the *a* positions of the A and C helices (pink) participate in both *trimeric* coiled-coil packing interactions. Note that the first and last *a* layers of the tetramer show knobs-into-holes packing between two helices.

(Figure 5). Note that each helix in the tetramer is tilted slightly about its axis, which effectively points the *b* residues of helix C and the *e* residues of helix D more toward the center of the structure, resulting in higher buried surface values at these sites.

In summary, while the GCN4-pVe structure conforms to the canonical knobs-into-holes interdigitation of hydrophobic residues in coiled coils, there are important differences. All the four triad core packing arrangements in the GCN4-pVe tetramer reveal that the $C^\alpha-C^\beta$ bond of each knob side chain makes an acute angle with the $C^\alpha-C^\alpha$ vector at the base of the recipient hole; this packing geometry is characteristic of classical trimeric coiled coils (*33*). Crick parametrization analysis indeed shows that the pitch, radius, and residues per turn of the GCN4-pVe tetramer are virtually identical to those of the GCN4-pII *trimer*, and differ greatly from those of the GCN4-pLI tetramer (Table 2). Remarkably, despite the formal tetramerization imposed by the *e* valine substitutions, the resulting architecture is a construct formed by two interlocking trimers.

Buried surface area (%)

	GCN4-pLI	GCN4-pVe			
	a-d core	*a-d* core		*a-d-e* core	
Positions		helix B	helix D	helix A	helix C
a	90	94	98	97	93
b	12	2	7	25	54
c	18	3	0	5	6
d	97	95	90	97	100
e	77	49	60	95	92
f	0	0	0	6	0
g	60	30	31	39	42

FIGURE 5: Buried surface areas in the parallel GCN4-pLI and GCN4-pVe tetramers. Percent buried surface area is expressed as the fraction of accessible side chain surface in the isolated helix that becomes buried in the parallel tetramer.

Comparison between Parallel GCN4-pVe and GCN4-pLI Tetramers. GCN4-pLI represents the archetypal model for parallel four-stranded coiled coils (*32*). The parallel tetrameric structure of GCN4-pVe reveals a different topology for this class of the coiled coil. We can summarize the major differences between the GCN4-pVe and GCN4-pLI structures as follows. (i) While the classical GCN4-pLI tetramer has approximate fourth-order rotational symmetry that dictates its square cross-section (*32*), GCN4-pVe lacks any such apparent symmetry and instead exhibits a rectangular cross section as a result of the unusual core packing arrangement (as a pair of conjoined *trimers*). (ii) Neighboring A−B and C−D helices of GCN4-pVe are offset by three amino acid residues with respect to each other. The translational helix offset is zero in the GCN4-pLI structure. (iii) In contrast to the alternating *a* and *d* layers in GCN4-pLI (*32*), GCN4-pVe shows an extremely tight-knit van der Waals packing extending beyond the *a* and *d* side chains. (iv) As a result of (iii), an axial channel that spans the length of the GCN4-pLI tetramer is much less pronounced in the structure of GCN4-pVe. Thus GCN4-pVe is significantly more tightly packed than GCN4-pLI. We should nonetheless emphasize that the surface area of each helix is less buried in GCN4-pVe (1425 Å^2 per helix) than in GCN4-pLI (1640 Å^2 per helix), due to the N- and C-terminal dimer overhangs in GCN4-pVe (see Figure 4).

Extending Crick's Principles for Parallel Tetramers. Together with our present results, it is now evident that van der Waals interactions beyond the canonical *a* and *d* side chains afford a variety of new coiled-coil assemblies (*2*, *75*−*77*). GCN4-pVe forms an unusual parallel coiled-coil tetramer with interhelical interactions that are unprecedented. This structure was unpredicted; indeed an initial goal of this work was to reproduce the interior packing of the antiparallel tetramerization domain seen in the *lac* repressor. It is noteworthy that the latter structure is based on three heptads, not five (*42*, *44*, *49*). How the number of heptads influences translational offsets between supercoiled α helices as well as their detailed packing interactions remains to be further explored.

Coiled coils are exceptional in that the symmetry and geometrical constraints amplify small differences in packing among side chains that contribute to formation of the hydrophobic core. This situation is seemingly at variance with studies that show that the interior of small globular proteins can be repacked quite freely with retention of the native fold (*78*). We suggest here that each of the four critical heptad positions in a coiled coil (*a*, *d*, *e*, and *g*) can play a determinative role in the final structure, depending on the number and presence of bulky or small nonpolar side chains that are present. In classical coiled coils, interactions between the *a* and *d* residues dominate the global fold, while *e* and *g* side chains are mostly polar, and often charged. If the *e* and/or *g* residues are valines or alanines, for example, new packing interactions become available, opening up higher-order helix−helix interacting possibilities that we see here and in previous reports (*45*). At this point we find it hard to predict how larger or smaller nonpolar side chains will behave at either the *e* or *g* positions. For example, do van der Waals interactions involving the *e* and *g* side chains dominate if the *a* and *d* positions include smaller nonpolar side chains such as alanine? More generally, when nonpolar side chains are present at any or all of the key *a*, *d*, *e*, or *g* positions, the combination that contains the most effective packing side chains might be expected to prevail. If so, additional distinctive heptad combinations should be possible, including triads such as *a*, *d*, *g*; *a*, *e*, *g*; and *d*, *e*, *g*; the inequivalence of each of the four positions (*a*, *d*, *e*, and *g*) suggests that these will not yield identical structures. Factors that control the helix offset, relative orientation, and homo-*versus* heteromeric composition all remain to be identified.

Implications for Coiled-Coil Structure and Prediction. Recent studies suggest that the range of potential coiled-coil structures is far greater than has been suspected, depending on the nature of the side chains at the *a* and *d* positions (*79*−*81*) as well as the presence of nonpolar side chains at the *e* and/or *g* positions (*45*−*47*). Defining the relative importance, selectivity, and context dependence of individual side chains at four hydrophobic positions in coiled coils presents a large experimental space for detailed investigation. In practice we know already that coiled-coil folding can yield a multiplicity of alternative conformations that are close in free energy, a situation that can result in intrinsic structural heterogeneity (*32*, *34*, *37*, *47*, *81*, *82*). Current design algorithms have difficulty discriminating among multiple configurations that are close in folding free energy, to ensure specificity in selecting a target conformation from a set of undesired competitors. A key issue in recent protein design efforts then is to achieve a balance between the requirements for stability and specificity (*18*, *31*). Havranek and Harbury attempted to take into account some of the diversity of alternative structures accessible to coiled-coil dimeric sequences (*27*).

Predictive rules for coiled-coil architecture have emphasized the *a*−*d* pair for obvious reasons (*83*). Analysis of a coiled-coil dodecamer structure points to a number of novel side chain−side chain packing combinations that remain to be tested (*39*, *75*). The variety of helix−helix interactions is evidently much greater than has been explored up to now, and additional experimental and theoretical studies will be needed to define and clarify the structural determinants of this interaction specificity. A comprehensive prediction algorithm will necessitate detailed understanding of the physical principles governing hydrophobic heptad-repeat patterns and coiled-coil assembly.

ACKNOWLEDGMENT

We thank John Schwanof at the National Synchrotron Light Source for support at beamline X4A, Xiuwen Ma for peptide purification, and Yingming Zhao for mass spectrometry analysis.

REFERENCES

1. Kohn, W. D., Mant, C. T., and Hodges, R. S. (1997) Alpha-helical protein assembly motifs, *J. Biol. Chem. 272*, 2583−2586.
2. Lupas, A. N., and Gruber, M. (2005) The structure of alpha-helical coiled coils, *Adv. Protein Chem. 70*, 37−78.
3. McLachlan, A. D., and Stewart, M. (1975) Tropomyosin coiled-coil interactions: evidence for an unstaggered structure, *J. Mol. Biol. 98*, 293−304.
4. Parry, D. A. (1982) Coiled-coils in alpha-helix-containing proteins: analysis of the residue types within the heptad repeat and the use of these data in the prediction of coiled-coils in other proteins, *Biosci. Rep. 2*, 1017−1024.
5. Lupas, A., Van Dyke, M., and Stock, J. (1991) Predicting coiled coils from protein sequences, *Science 252*, 1162−1164.
6. Hodges, R. S., Sodek, J., Smillie, L. B., and Jurasek, L. (1972) Tropomyosin: amino acid sequence and coiled-coil structure, *Cold Spring Harbor Symp. Quant. Biol. 37*, 299−310.
7. Crick, F. H. C. (1953) The packing of α-helices: simple coiled-coils, *Acta Crystallogr. 6*, 689−697.
8. O'Shea, E. K., Klemm, J. D., Kim, P. S., and Alber, T. (1991) X-ray structure of the GCN4 leucine zipper, a two-stranded, parallel coiled coil, *Science 254*, 539−544.
9. Betz, S. F., Bryson, J. W., and DeGrado, W. F. (1995) Native-like and structurally characterized designed alpha-helical bundles, *Curr. Opin. Struct. Biol. 5*, 457−463.
10. O'Shea, E. K., Lumb, K. J., and Kim, P. S. (1993) Peptide 'Velcro': Design of a heterodimeric coiled coil, *Curr. Biol. 3*, 658−667.
11. Krylov, D., Mikhailenko, I., and Vinson, C. (1994) A thermodynamic scale for leucine zipper stability and dimerization specificity: e and g interhelical interactions, *EMBO J. 13*, 2849−2861.
12. Monera, O. D., Kay, C. M., and Hodges, R. S. (1994) Electrostatic interactions control the parallel and antiparallel orientation of alpha-helical chains in two-stranded alpha-helical coiled-coils, *Biochemistry 33*, 3862−3871.
13. Zeng, X., Zhu, H., Lashuel, H. A., and Hu, J. C. (1997) Oligomerization properties of GCN4 leucine zipper e and g position mutants, *Protein Sci. 6*, 2218−2226.
14. Kohn, W. D., Kay, C. M., and Hodges, R. S. (1998) Orientation, positional, additivity, and oligomerization-state effects of interhelical ion pairs in alpha-helical coiled-coils, *J. Mol. Biol. 283*, 993−1012.
15. McClain, D. L., Binfet, J. P., and Oakley, M. G. (2001) Evaluation of the energetic contribution of interhelical Coulombic interactions for coiled coil helix orientation specificity, *J. Mol. Biol. 313*, 371−383.
16. Zhou, N. E., Kay, C. M., and Hodges, R. S. (1994) The role of interhelical ionic interactions in controlling protein folding and stability. De novo designed synthetic two-stranded alpha-helical coiled-coils, *J. Mol. Biol. 237*, 500−512.
17. Graddis, T. J., Myszka, D. G., and Chaiken, I. M. (1993) Controlled formation of model homo- and heterodimer coiled coil polypeptides, *Biochemistry 32*, 12664−12671.
18. Moll, J. R., Ruvinov, S. B., Pastan, I., and Vinson, C. (2001) Designed heterodimerizing leucine zippers with a ranger of pIs and stabilities up to 10(-15) M, *Protein Sci. 10*, 649−655.
19. Lupas, A. (1997) Predicting coiled-coil regions in proteins, *Curr. Opin. Struct. Biol. 7*, 388−393.
20. Wolf, E., Kim, P. S., and Berger, B. (1997) MultiCoil: a program for predicting two- and three-stranded coiled coils, *Protein Sci. 6*, 1179−1189.
21. Woolfson, D. N., and Alber, T. (1995) Predicting oligomerization states of coiled coils, *Protein Sci. 4*, 1596−1607.
22. Berger, B., Wilson, D. B., Wolf, E., Tonchev, T., Milla, M., and Kim, P. S. (1995) Predicting coiled coils by use of pairwise residue correlations, *Proc. Natl. Acad. Sci. U.S.A. 92*, 8259−8263.
23. Conway, J. F., and Parry, D. A. (1990) Structural features in the heptad substructure and longer range repeats of two-stranded alpha-fibrous proteins, *Int. J. Biol. Macromol. 12*, 328−334.
24. Conway, J. F., and Parry, D. A. (1991) Three-stranded alpha-fibrous proteins: the heptad repeat and its implications for structure, *Int. J. Biol. Macromol. 13*, 14−16.
25. Zitzewitz, J. A., Bilsel, O., Luo, J., Jones, B. E., and Matthews, C. R. (1995) Probing the folding mechanism of a leucine zipper peptide by stopped-flow circular dichroism spectroscopy, *Biochemistry 34*, 12812−12819.
26. Krantz, B. A., and Sosnick, T. R. (2001) Engineered metal binding sites map the heterogeneous folding landscape of a coiled coil, *Nat. Struct. Biol. 8*, 1042−1047.
27. Havranek, J. J., and Harbury, P. B. (2003) Automated design of specificity in molecular recognition, *Nat. Struct. Biol. 10*, 45−52.
28. DeGrado, W. F., Summa, C. M., Pavone, V., Nastri, F., and Lombardi, A. (1999) De novo design and structural characterization of proteins and metalloproteins, *Annu. Rev. Biochem. 68*, 779−819.
29. Hodges, R. S. (1996) Boehringer Mannheim award lecture 1995. La conference Boehringer Mannheim 1995. De novo design of alpha-helical proteins: basic research to medical applications, *Biochem. Cell Biol. 74*, 133−154.
30. Harbury, P. B., Plecs, J. J., Tidor, B., Alber, T., and Kim, P. S. (1998) High-resolution protein design with backbone freedom, *Science 282*, 1462−1467.
31. Bryson, J. W., Betz, S. F., Lu, H. S., Suich, D. J., Zhou, H. X., O'Neil, K. T., and DeGrado, W. F. (1995) Protein design: a hierarchic approach, *Science 270*, 935−941.
32. Harbury, P. B., Zhang, T., Kim, P. S., and Alber, T. (1993) A switch between two-, three-, and four-stranded coiled coils in GCN4 leucine zipper mutants, *Science 262*, 1401−1407.
33. Harbury, P. B., Kim, P. S., and Alber, T. (1994) Crystal structure of an isoleucine-zipper trimer, *Nature 371*, 80−83.
34. Gonzalez, L., Jr., Brown, R. A., Richardson, D., and Alber, T. (1996) Crystal structures of a single coiled-coil peptide in two oligomeric states reveal the basis for structural polymorphism, *Nat. Struct. Biol. 3*, 1002−1009.
35. Gonzalez, L., Jr., Woolfson, D. N., and Alber, T. (1996) Buried polar residues and structural specificity in the GCN4 leucine zipper, *Nat. Struct. Biol. 3*, 1011−1018.
36. Gonzalez, L., Jr., Plecs, J. J., and Alber, T. (1996) An engineered allosteric switch in leucine-zipper oligomerization, *Nat. Struct. Biol. 3*, 510−515.
37. Akey, D. L., Malashkevich, V. N., and Kim, P. S. (2001) Buried polar residues in coiled-coil interfaces, *Biochemistry 40*, 6352−6360.
38. Harbury, P. B., Tidor, B., and Kim, P. S. (1995) Repacking protein cores with backbone freedom: structure prediction for coiled coils, *Proc. Natl. Acad. Sci. U.S.A. 92*, 8408−8412.
39. North, B., Summa, C. M., Ghirlanda, G., and DeGrado, W. F. (2001) D(n)-symmetrical tertiary templates for the design of tubular proteins, *J. Mol. Biol.* 311, 1081−1090.
40. Ho, S. P., and DeGrado, W. F. (1987) Design of a 4-helix bundle protein: synthesis of peptides which self-associate into a helical protein, *J. Am. Chem. Soc. 109*, 6751−6758.
41. Alberti, S., Oehler, S., von Wilcken-Bergmann, B., and Muller-Hill, B. (1993) Genetic analysis of the leucine heptad repeats of Lac repressor: evidence for a 4-helical bundle, *EMBO J. 12*, 3227−3236.
42. Fairman, R., Chao, H. G., Mueller, L., Lavoie, T. B., Shen, L., Novotny, J., and Matsueda, G. R. (1995) Characterization of a new four-chain coiled-coil: influence of chain length on stability, *Protein Sci. 4*, 1457−1469.
43. Fairman, R., Chao, H. G., Lavoie, T. B., Villafranca, J. J., Matsueda, G. R., and Novotny, J. (1996) Design of heterotetrameric coiled coils: evidence for increased stabilization by Glu(-)-Lys(+) ion pair interactions, *Biochemistry 35*, 2824−2829.
44. Solan, A., Ratia, K., and Fairman, R. (2002) Exploring the role of alanine in the structure of the Lac repressor tetramerization domain, a ferritin-like Alacoil, *J. Mol. Biol. 317*, 601−612.
45. Liu, J., Zheng, Q., Deng, Y., Cheng, C. S., Kallenbach, N. R., and Lu, M. (2006) A seven-helix coiled coil, *Proc. Natl. Acad. Sci. U.S.A. 103*, 15457−15462.
46. Deng, Y., Liu, J., Zheng, Q., Eliezer, D., Kallenbach, N. R., and Lu, M. (2006) Antiparallel four-stranded coiled coil specified by a 3-3-1 hydrophobic heptad repeat, *Structure 14*, 247−255.
47. Yadav, M. K., Leman, L. J., Price, D. J., Brooks Iii, C. L., Stout, C. D., and Ghadiri, M. R. (2006) Coiled coils at the edge of configurational heterogeneity. Structural analyses of parallel and antiparallel homotetrameric coiled coils reveal configurational

sensitivity to a single solvent-exposed amino acid substitution, *Biochemistry 45*, 4463−4473.
48. Yadav, M. K., Redman, J. E., Leman, L. J., Alvarez-Gutierrez, J. M., Zhang, Y., Stout, C. D., and Ghadiri, M. R. (2005) Structure-based engineering of internal cavities in coiled-coil peptides, *Biochemistry 44*, 9723−9732.
49. Friedman, A. M., Fischmann, T. O., and Steitz, T. A. (1995) Crystal structure of lac repressor core tetramer and its implications for DNA looping, *Science 268*, 1721−1727.
50. Deng, Y., Liu, J., Zheng, Q., Yong, W., and Lu, M. (2006) Structures and polymorphic interactions of two heptad-repeat regions of the SARS virus S2 protein, *Structure 14*, 889−899.
51. Gernert, K. M., Surles, M. C., Labean, T. H., Richardson, J. S., and Richardson, D. C. (1995) The Alacoil: a very tight, antiparallel coiled-coil of helices, *Protein Sci. 4*, 2252−2260.
52. Banner, D. W., Kokkinidis, M., and Tsernoglou, D. (1987) Structure of the ColE1 rop protein at 1.7 Å resolution, *J. Mol. Biol. 196*, 657−675.
53. Lu, M., Shu, W., Ji, H., Spek, E., Wang, L., and Kallenbach, N. R. (1999) Helix capping in the GCN4 leucine zipper, *J. Mol. Biol. 288*, 743−752.
54. Kunkel, T. A., Roberts, J. D., and Zakour, R. A. (1987) Rapid and efficient site-specific mutagenesis without phenotypic selection, *Methods Enzymol. 154*, 367−382.
55. Edelhoch, H. (1967) Spectroscopic determination of tryptophan and tyrosine in proteins, *Biochemistry 6*, 1948−1954.
56. Chen, Y. H., Yang, J. T., and Chau, K. H. (1974) Determination of the helix and beta form of proteins in aqueous solution by circular dichroism, *Biochemistry 13*, 3350−3359.
57. Cantor, C., and Schimmel, P. (1980) *Biophysical Chemistry*, Vol. III, W. H. Freeman and Co., New York.
58. Shu, W., Ji, H., and Lu, M. (1999) Trimerization specificity in HIV-1 gp41: analysis with a GCN4 leucine zipper model, *Biochemistry 38*, 5378−5385.
59. Johnson, M. L., Correia, J. J., Yphantis, D. A., and Halvorson, H. R. (1981) Analysis of data from the analytical ultracentrifuge by nonlinear least-squares techniques, *Biophys. J. 36*, 575−588.
60. Laue, T. M., Shah, B. D., Ridgeway, T. M., and Pelletier, S. L. (1992) in *Analytical Ultracentrifugation in Biochemistry and Polymer Science* (Harding, S. E., Rowe, A. J., and Horton, J. C., Eds.) pp 90−125, Royal Society of Chemistry, Cambridge.
61. Otwinowski, Z., and Minor, W. (1997) Processing X-ray diffraction data collected in oscillation mode, *Methods Enzymol. 276*, 307−326.
62. Storoni, L. C., McCoy, A. J., and Read, R. J. (2004) Likelihood-enhanced fast rotation functions, *Acta Crystallogr. D Biol. Crystallogr. 60*, 432−438.
63. Lamzin, V. S., and Wilson, K. S. (1993) Automated refinement of protein models, *Acta Crystallogr. D 49*, 129−149.
64. Murshudov, G. N., Vagin, A. A., and Dodson, E. J. (1997) Refinement of macromolecular structures by the maximum-likehood method, *Acta Crystallogr. D 53*, 240−255.
65. Potterton, E., Briggs, P., Turkenburg, M., and Dodson, E. (2003) A graphical user interface to the CCP4 program suite, *Acta Crystallogr. D Biol. Crystallogr. 59*, 1131−1137.
66. Jones, T. A., Zou, J. Y., Cowan, S. W., and Kjeldgaard, M. (1991) Improved methods for building protein models in electron density maps and the location of errors in these models, *Acta Crystallogr. A 47*, 110−119.
67. Schomaker, V., and Trueblood, K. N. (1998) Correlation of internal torsional motion with overall molecular motion in crystals, *Acta Crystallogr. B 54*, 507−514.
68. Strelkov, S. V., and Burkhard, P. (2002) Analysis of alpha-helical coiled coils with the program TWISTER reveals a structural mechanism for stutter compensation, *J. Struct. Biol. 137*, 54−64.
69. Brunger, A. T., Adams, P. D., Clore, G. M., DeLano, W. L., Gros, P., Grosse-Kunstleve, R. W., Jiang, J. S., Kuszewski, J., Nilges, M., Pannu, N. S., Read, R. J., Rice, L. M., Simonson, T., and Warren, G. L. (1998) Crystallography & NMR system: A new software suite for macromolecular structure determination, *Acta Crystallogr. D Biol. Crystallogr. 54*, 905−921.
70. Eisenberg, D., and McLachlan, A. D. (1986) Solvation energy in protein folding and binding, *Nature 319*, 199−203.
71. Evans, S. V. (1993) SETOR: hardware-lighted three-dimensional solid model representations of macromolecules, *J. Mol. Graph 11*, 134−138.
72. Nicholls, A., Sharp, K. A., and Honig, B. (1991) Protein folding and association: insights from the interfacial and thermodynamic properties of hydrocarbons, *Proteins 11*, 281−296.
73. Lovell, S. C., Word, J. M., Richardson, J. S., and Richardson, D. C. (2000) The penultimate rotamer library, *Proteins 40*, 389−408.
74. Ponder, J. W., and Richards, F. M. (1987) Tertiary templates for proteins. Use of packing criteria in the enumeration of allowed sequences for different structural classes, *J. Mol. Biol. 193*, 775−791.
75. Calladine, C. R., Sharff, A., and Luisi, B. (2001) How to untwist an alpha-helix: structural principles of an alpha-helical barrel, *J. Mol. Biol. 305*, 603−618.
76. Koronakis, V., Sharff, A., Koronakis, E., Luisi, B., and Hughes, C. (2000) Crystal structure of the bacterial membrane protein TolC central to multidrug efflux and protein export, *Nature 405*, 914−919.
77. Walshaw, J., and Woolfson, D. N. (2001) Socket: a program for identifying and analysing coiled-coil motifs within protein structures, *J. Mol. Biol. 307*, 1427−1450.
78. Mooers, B. H., Datta, D., Baase, W. A., Zollars, E. S., Mayo, S. L., and Matthews, B. W. (2003) Repacking the Core of T4 lysozyme by automated design, *J. Mol. Biol. 332*, 741−756.
79. Liu, J., Yong, W., Deng, Y., Kallenbach, N. R., and Lu, M. (2004) Atomic structure of a tryptophan-zipper pentamer, *Proc. Natl. Acad. Sci. U.S.A. 101*, 16156−16161.
80. Liu, J., Zheng, Q., Deng, Y., Kallenbach, N. R., and Lu, M. (2006) Conformational transition between four and five-stranded phenylalanine Zippers determined by a local packing interaction, *J. Mol. Biol. 361*, 168−179.
81. Slovic, A. M., Stayrook, S. E., North, B., and Degrado, W. F. (2005) X-ray structure of a water-soluble analog of the membrane protein phospholamban: sequence determinants defining the topology of tetrameric and pentameric coiled coils, *J. Mol. Biol. 348*, 777−787.
82. Lovejoy, B., Choe, S., Cascio, D., McRorie, D. K., DeGrado, W. F., and Eisenberg, D. (1993) Crystal structure of a synthetic triple-stranded alpha-helical bundle, *Science 259*, 1288−1293.
83. Walshaw, J., and Woolfson, D. N. (2003) Extended knobs-into-holes packing in classical and complex coiled-coil assemblies, *J. Struct. Biol. 144*, 349−361.

BI061914M